




Letter

Active real-time control of Alfvén eigenmodes by neutral beam and electron cyclotron heating in the DIII-D tokamak

Wenhui Hu^{1,2,a} , K.E.J. Olofsson³ , A.S. Welander³, W.W. Heidbrink⁴ ,
M.A. Van Zeeland³, M.E. Austin⁵, C.S. Collins³, D.A. Humphreys³,
E. Kolemen⁶, Jiangang Li¹, Bingjia Xiao¹ and DIII-D Team³

¹ Institute of Plasma Physics, Chinese Academy of Science, Hefei, Anhui 230031, People's Republic of China

² University of Science and Technology of China, Hefei, Anhui 230026, People's Republic of China

³ General Atomics, PO Box 85608, San Diego, CA 92186-5608, United States of America

⁴ Department of Physics and Astronomy, University of California, Irvine, CA 92697, United States of America

⁵ University of Texas-Austin, Austin, TX 78712, United States of America

⁶ Princeton University, Princeton, NJ 08544, United States of America

E-mail: huwh@ipp.ac.cn

Received 5 July 2018, revised 14 August 2018

Accepted for publication 30 August 2018

Published 17 September 2018



Abstract

A real-time Alfvén eigenmode (AE) controller is designed and implemented for the first time in DIII-D. The experimental test consists of two parts: (i) open-loop and feedback control using neutral beam power as an actuator and (ii) open-loop control using electron cyclotron heating (ECH) as an actuator. Part (i) demonstrates the feasibility of varying neutral beam power injected into plasma to control overall AE amplitude as well as the successful application of real-time electron cyclotron emission (ECE) as the process controller's AE amplitude sensor. The temporal evolution of AE amplitude at a specific radial location has also been controlled by selecting a subset of the radial ECE array. Part (ii) finds a complicated dependence of AE evolution on ECH power and more dedicated investigation is needed to explore the dynamical ECH-control model. Additionally, the ratio between TRANSP calculated neutron rate and measured neutron rate is found to correspond closely with AE amplitudes in discharges with feedback control, verifying that this ratio can be another sensor for the control system.

Keywords: Alfvén eigenmode, feedback control, real-time control, ECRH, NBI, ECE

(Some figures may appear in colour only in the online journal)

Introduction

Energetic particles (EP) play a major role in fusion reactor self-heating, external heating, momentum input and current drive [1]. Several studies show that the presence of

multiple-overlapping Alfvén eigenmodes (AEs) can cause orbit stochasticity and confinement degradation of fast ions [2–9] leading to heating and current drive efficiency reduction, a neutron production/fusion yield deficit [10–14], and damage to the first wall [15, 16]. But appreciable transport of fast ions can be avoided if AE amplitudes can be kept below a threshold level [12, 17]. Alternatively, an intermediate level of

^a Author to whom any correspondence should be addressed.

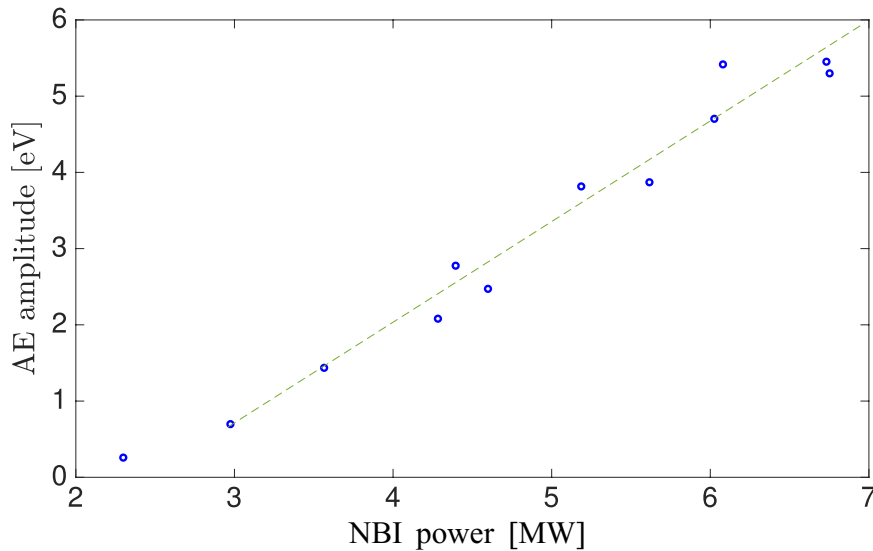


Figure 1. Average AE amplitude measured by ECE versus total beam power in $B_T = 2$ T, L-mode current ramp experiments.

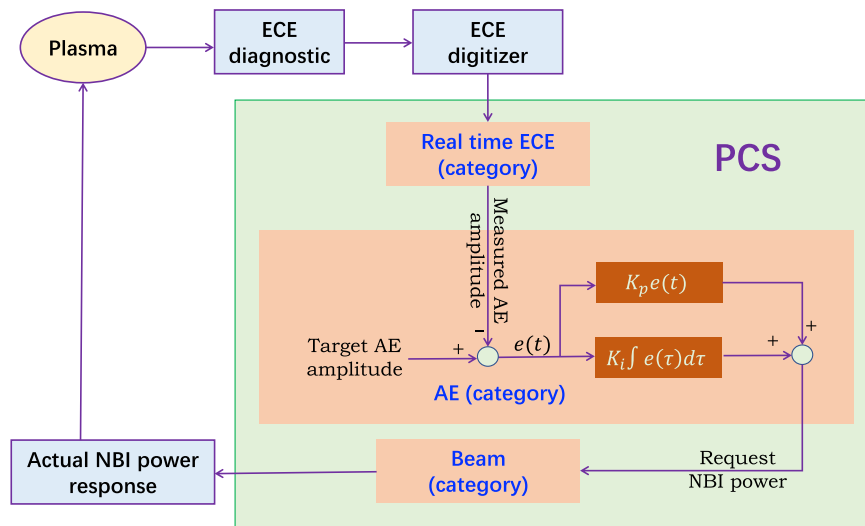


Figure 2. Diagram of the proportional-integral AE control system in the DIII-D PCS. ‘Category’ refers to different functional areas in the PCS software architecture that enable both operators and control designers to organize control operations by relevant actuators, diagnostics, or control goals.

AEs may even be favorable for plasma performance. Studies find that formation of edge and internal transport barriers can be triggered by Alfvén waves [18–21]. Additionally, some level of pressure profile flattening could reduce susceptibility to large scale MHD instability. Controlling AEs at a non-zero level which optimizes fast-ion heating and current drive efficiency while avoiding excessive fast ion losses may be quite beneficial for a fusion reactor. One mission (goal) of non-axisymmetric control for the ITER plasma control system (PCS) is controlling AEs in high performance plasmas to maintain fusion burn and avoid damage to the first wall [22, 23].

Searching for possible actuators to control AEs has been an active area of research both in tokamaks and stellarators. Central electron cyclotron current drive (ECCD) is found to suppress AE activity in Heliotron J [24] and in steady-state hybrid scenarios of DIII-D [25]. Electron cyclotron heating (ECH) injected near the minimum in the safety factor profile, $q = q_{\min}$ is found to change behavior of AEs dramatically

in DIII-D [26–29] and ASDEX-U [30], while ECH injected on-axis suppressed AEs in the TJ-II stellarator [31]. Neutral beam voltage variation experiments in DIII-D show promise for control of AEs [32] and outboard injection of neutral beams in NSTX-U has suppressed higher frequency AEs [33]. Externally applied static 3D fields are also possible actuators to mitigate AE activity as demonstrated in NSTX [34, 35] and ASDEX-U [36]. Lower hybrid waves were theoretically calculated to be capable of suppressing α particle-driven AEs [37]. High harmonic fast wave heating has also been experimentally shown to suppress the AEs in NSTX [38].

Reversed shear Alfvén eigenmodes (RSAE) and toroidal Alfvén eigenmodes (TAE) have been extensively studied in DIII-D in the current ramp up phase, when incomplete current penetration results in high central safety factor and strong drive due to enhanced coupling to multiple higher order resonances [11, 12, 17, 26–28, 32, 39, 40, 43]. The DIII-D electron cyclotron emission (ECE) diagnostic, with 40 low noise

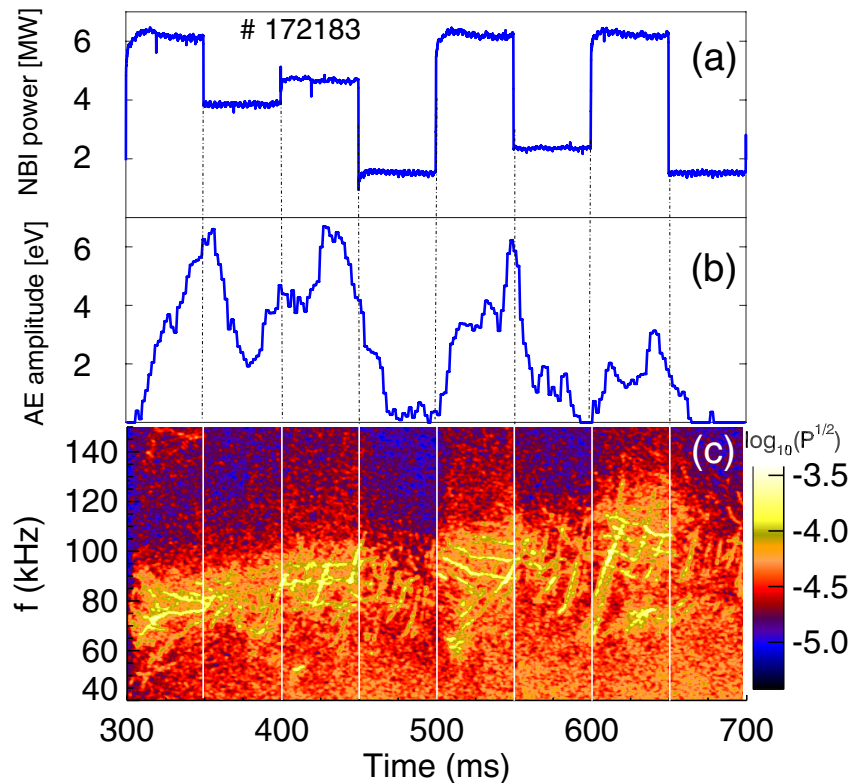


Figure 3. Discharge 172183. (a) Pre-programmed NBI power, (b) AEs amplitude represented by electron temperature measured by ECE, (c) CO₂ interferometer cross power spectrum.

radially spaced channels across the plasma midplane [41], is ideally suited to measure the structure and amplitude of AEs [42]. Neutral beam injection (NBI) power scan experiments show that AE amplitude and fast-ion transport begin to increase proportionally with beam power when the power is above a threshold of approximately 3 MW [12, 17] in ~ 2 Tesla DIII-D current ramp experiments. Figure 1 shows that the AE amplitude in a set of oval-shaped, low-confinement (L-mode) discharges during the ramp scales linearly with NBI power when the power is above 3 MW. The line-averaged density for these discharges are $n_e \approx 2.5\text{--}2.9 \times 10^{13} \text{ cm}^{-3}$, $B_T = 2.05$ T and the plasma current ramps to $I_p = 800$ kA at 600 ms. The AE amplitude is taken from ECE-detected electron temperature fluctuations. In figure 1, the AE amplitude is represented by the mean value of the coherent power spectral density from Fourier analysis of temperature measurements from ten pairs of ECE channels with a bandpass between the geodesic acoustic and TAE frequencies (which is approximately within 50–200 kHz), averaged over the period of $t = 400\text{--}700$ ms. The ten ECE pairs are made up of channels (1, 2), (3, 4), (5, 6) (19, 20) that span from $\rho = 1$ to $\rho = 0.1$, where ρ is the normalized square root of toroidal flux. Based on this property, a linear feedback controller can be built using NBI power as an actuator to control the AE amplitude.

In this Letter we report the first active real-time control of Alfvén eigenmodes in a tokamak. The demonstration utilizes a new dedicated AE module in the DIII-D plasma control system (PCS). Neutral beam power variation and ECH are used as actuators to control the AEs and radially localized ECE

measurements are used to monitor and obtain a given temporally varying AE target amplitude.

The real-time AE control system

The design of the AE control system is based on real-time ECE (rt-ECE) measurements through which the Alfvén activity is monitored during a discharge by the plasma control system. The sampling frequency for the ECE diagnostic is 500 kHz and the rt-ECE digitizer produces 341 complete sample sets (40 ECE channels per set) acquired over a 682 μs time period, which are immediately sent to the plasma control system (PCS) for analysis. This means 1024 samples of ECE measurements every 2048 μs are accessible to the PCS for each one of the 40 ECE channels that are located along the horizontal radius of the tokamak. The AE amplitude from core to edge can be obtained in real-time by doing windowed Fourier transforms for all ECE channels and summing up the spectral power with coherence higher than a target value in a given bandwidth. Here, 80% is used for the target coherence and modes between 50–200 kHz (as in figure 1) are monitored since that frequency range corresponds roughly to the range in which RSAEs and TAEs are observed in the target plasmas. In the DIII-D PCS a new ECE category is implemented to calculate the AE amplitude in real-time. Here a control ‘category’ is a function in the PCS that roughly corresponds to an actuator or class of actuators (e.g. NBI) and corresponding feedback control algorithms. A proportional-integral (PI) controller

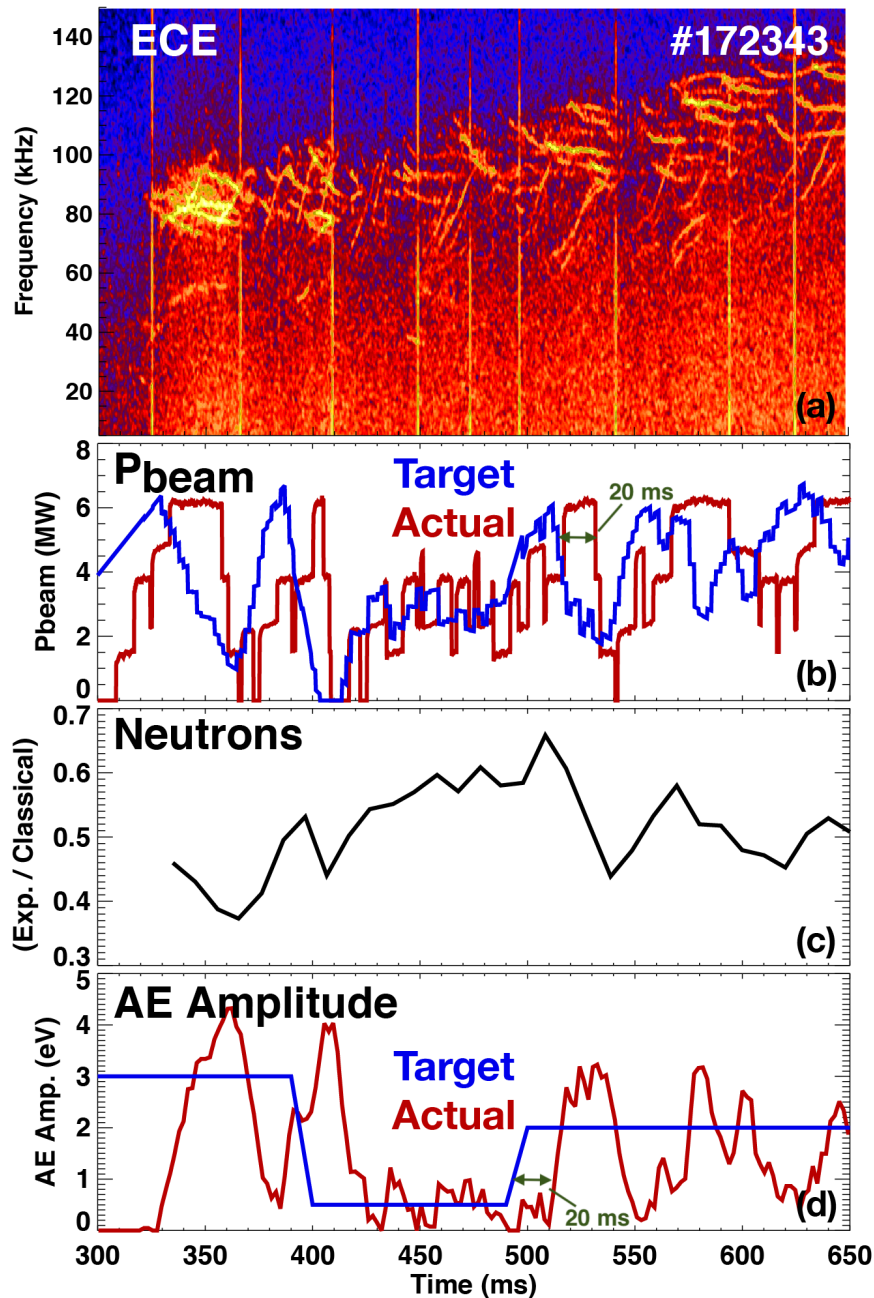


Figure 4. Discharge 172343. (a) ECE spectrum, (b) AE controller requested NBI power (blue line) and actual response NBI power (red line), (c) measured neutrons production rate over TRANSP predicted classical neutrons production rate and (d) target AE amplitude (blue line) and real-time ECE measured AE amplitude (red line).

using NBI power as the actuator is built within the AE control category that gives beam power commands/requests to the beam category according to the PI controller output. The beam category algorithm then calculates how each beam should act to provide the requested beam power and adjusts the necessary beam command. The AE control system architecture is shown in figure 2.

To test the open-loop behavior of the system, i.e. not feeding back on the measured amplitudes, NBI power corresponding to different pre-programmed waveforms is applied and the overall AE level is monitored. The target discharges are inner wall limited, oval-shaped, L-mode plasmas in the

current ramp up phase with $B_T = 2.04$ T. For these discharges the line-averaged density ramps from $n_e = 1.5 \times 10^{13} \text{ cm}^{-3}$ to $2.5 \times 10^{13} \text{ cm}^{-3}$ at 700 ms and plasma current ramps to $I_p = 800$ kA at 600 ms. Figure 3 is an example of an open-loop response discharge, in which the total NBI power provided by the sum of three co-injected deuterium neutral beams with constant energy of 81 keV or 75 keV is varied between 1.5–6.2 MW (figure 3(a)). Figure 3(b) shows time evolution of AE amplitude represented by ECE temperature measurements. The same ECE channels and pairs as in figure 1 are used to calculate real-time AE amplitude. AE activity is also shown in figure 3(c) which displays density fluctuation data

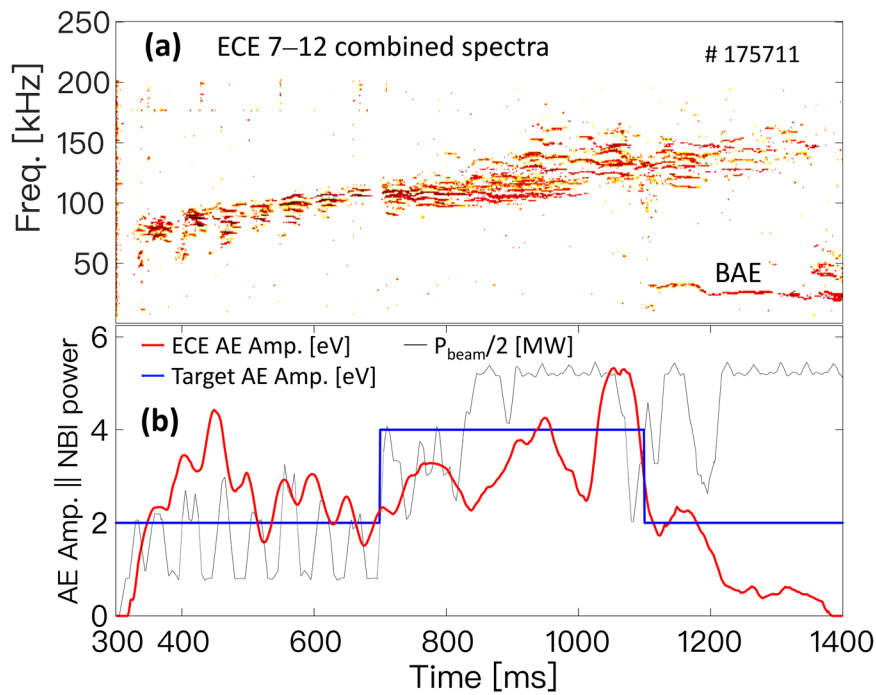


Figure 5. Discharge 175711. (a) Combined spectra of ECE channels 7–12. (b) Target AE amplitude (blue line) and real-time ECE (channel 7–12) measured AE amplitude (red line). The black line is the total beam power injected into plasma.

from a cross-power spectrum of a vertical and radial CO_2 interferometer chord. Figure 3 shows that both ECE and CO_2 interferometer-detected AE amplitudes grow when NBI power is high and decrease when NBI power becomes low, except that the overall AE amplitude has a tendency to decrease as the current increases and penetrates due to both increasing damping and reduced drive [43].

Control of global AE amplitudes using modulated NBI power

A feedback control discharge that attempts to drive the AE amplitude to track a varying target value is shown in figure 4. Figure 4(a) shows the ECE spectrum evolution. Figure 4(d) gives the target AE amplitude (blue) and the actual AE amplitude (red). On average the AE amplitude follows the target with a delay of about 20 ms. This delay is caused by the lag in the actual NBI power response to the NBI power command/request which is also around 20 ms, as shown in figure 4(b). The reason for this delay comes primarily from two parts. The first part is that for this discharge three neutral beams are used as actuators and the algorithm used in the beam category in figure 2 is changing their injected power by changing the duty-cycle of each beam. Each beam injects one pulse in one averaging time interval. The average power for the beam over that interval is the product of the power available for the beam and the duty-cycle of the beam averaged over a specified time interval. The averaging interval for three neutral beams is set to be 25 ms which is the shortest time that could be used reliably. This means that each beam is fired for a length of time between 0 and 25 ms. The duration of the next pulse is calculated using the present value of the commanded

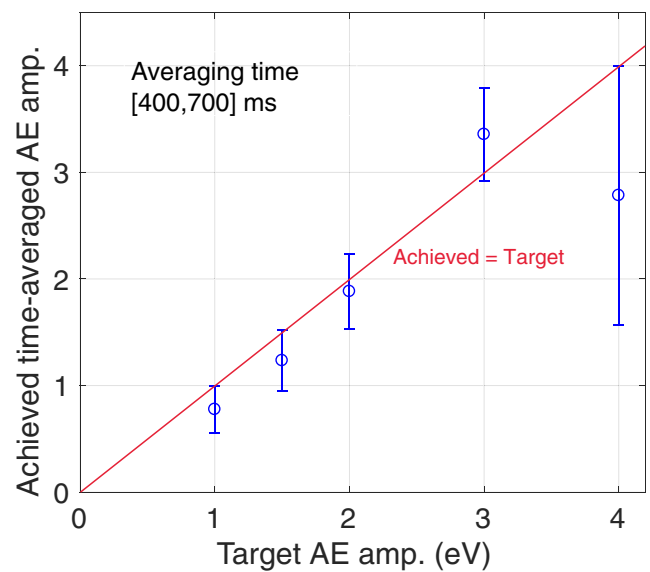


Figure 6. Time-averaged target AE level and mean time-averaged achieved AE level during 400–700 ms in experiments (blue dot) with error bars representing the mean deviation between the achieved and target AE. The red line is plotted as reference line showing achieved AE level equals target AE level.

neutral beam power. The power injected from one beam needs to be considered as an average over each 25 ms interval, so there is roughly a 25/2 ms delay between the power command and the average power achieved. Another factor contributing to the latency is that in order to avoid having all of the beams turning on or off at the same time, by default the start time of the averaging interval for each beam is shifted with respect to the start time of the averaging intervals for the other beams. In the experiment because

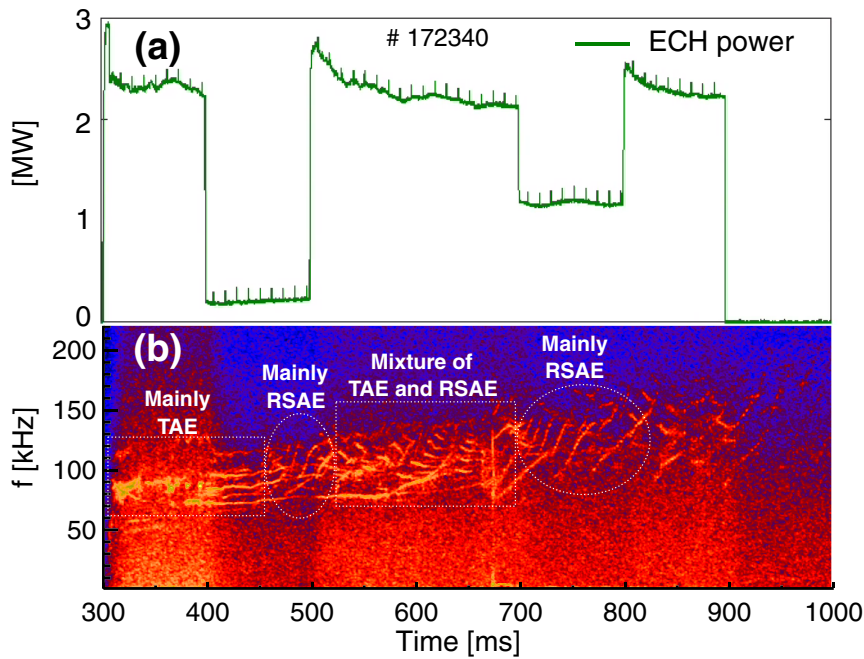


Figure 7. Discharge 172340. (a) Pre-programmed ECH power waveform and (b) cross power of adjacent ECE channels that are located near q_{\min} .

three neutral beams are used under PCS control, the start times can be shifted by 25/3 ms with respect to each other. This effect can therefore contribute a further difference between the command beam timing and the actual timing of about 8.3 ms, particularly when the power is rapidly ramping down or up.

The measured neutron production rate for the feedback control discharge is compared with the TRANSP calculated classical neutron production rate, and the ratio between them is plotted in figure 4(c). As expected, the ratio is shown to change inversely with the AE amplitude, which is similar to the statistical results obtained from a series of different discharges in DIII-D [8, 9]. This is consistent with the idea that as an alternative to measured AE amplitudes, the ratio of diagnostic/TRANSP neutron rate can be a viable and useful sensor for the AE controller [8]. A non-trivial requirement for this to be implemented, however, is a model that can calculate the neutron rate sufficiently fast. Such an algorithm is under development [44] and will be implemented as an option in an updated controller version.

Control of local AE amplitude using modulated NBI power

Since there are multiple ECE channels distributed from the plasma edge to the axis, it is possible to extend the control algorithm to target a radially localized AE amplitude waveform by carrying out the rt-ECE fluctuation analysis with a subset of the ECE array corresponding to this radial location. Figure 5 shows results from an active feedback case in which the AE amplitude in the range $\rho \approx 0.4$ – 0.7 is made to

hit a target waveform by using only ECE channels 7–12. In this discharge, the plasma current ramps up to 1200 kA at 2000 ms, which is a much slower ramp speed compared with the discharge presented in figure 4. Figure 5 shows the AE amplitude is maintained at the target level before 1200 ms. After 1200 ms, however, an interesting and unexpected series of events take place. First, beta-induced Alfvén eigenmodes (BAE) outside of the 50–200 kHz range of the amplitude monitor bandpass range appear followed by a reduction in TAE amplitudes. It is conjectured that somehow, the unstable BAEs cause transport of fast particles which are responsible for driving the higher frequency AEs inside of the bandpass. This in turn could reduce the drive for the higher frequency AEs and cause the controller to not reach the programmed AE target values even with increased NBI power (black line in figure 5(b)). Since the modes are different frequencies as well as different toroidal mode numbers and all are driven by multiple higher order resonances with finite width, the nonlinear phase space interaction which leads to this process is complicated, outside the scope of this study and will be left for a further more detailed analysis.

What is more, figures 4 and 5 are representative of feedback control results. Active feedback using NBI was attempted in 16 discharges with various targets. The mean value of achieved time-averaged AE amp. and time-averaged target AE amp. for these discharges is in plotted in figure 6. It compares the target AE amplitude with the achieved AE amplitude for 16 discharges with different target waveforms between 400–700 ms. The error bars represent the mean deviation between the achieved and target AE. On average, the achieved value is close to the target value but deviations from the target as large as ~30% are often observed.

Testing of ECH as a real-time AE actuator

Motivated by previous results showing a large impact of ECH on AEs in several devices worldwide [22–27], the suitability of ECH as an actuator in the PCS AE controller was tested. For these preliminary tests, a pre-programmed waveform was used in open loop mode and the AE amplitude was monitored. The pre-programmed ECH power waveform used is shown in figure 7(a) and this waveform is applied to a similar oval shaped plasma in the current ramp up phase from $t = 300$ ms at the same time constant NBI power of 4.7 MW is injected. The ECH is injected at q_{\min} near the plasma mid-radius. The ECE spectrum in figure 7(b) shows the evolution of the AE amplitude with ECH power variation at $\rho \approx 0.45$ where q_{\min} is near. The process is divided into five stages. (i) At $t = 300$ ms, ECH power is 2.3 MW and mainly the TAEs grow and persist until $t = 400$ ms. (ii) At 400 ms, ECH power is decreased to 0.2 MW and reversed shear Alfvén eigenmodes start to grow. After 450 ms, there are mainly RSAEs. (iii) At 500 ms, when the ECH power is increased again, TAEs reappear and a mixture of RSAEs and TAEs appears during the $t = 500$ –700 ms period. (iv) After 700 ms, when the ECH power decreases again, TAEs vanish and RSAEs become dominant. (v) After 900 ms, the AE activity gradually decreases because the drive is decreasing rapidly as the current penetrates until a point at which the damping becomes larger than the driving force [43]. The above process shows a clear impact of the ECH on AEs but the actual AE level versus ECH power is much more complicated than that shown in figure 1 for NBI power. These results are consistent with simulations and observations presented in [28] which show that both TAE and RSAE amplitudes and their localization change with dramatically with ECH power. More work is required to effectively utilize ECH as a plausible actuator in the PCS AE controller.

Conclusions and future work

An AE control scheme has been implemented and undergone initial testing in the DIII-D plasma control system. These results mark the first step towards feedback control of AEs, not only for reducing their harmful effects, but potentially to optimize discharge performance. The injected neutral beam power in conjunction with a real-time ECE diagnostic system that detects AE amplitudes has been used as a proof-of-principle actuator to control both global AE levels as well as AE levels at a given radius. Pre-programmed ECH power waveforms combined with NBI heating creates a complicated evolution of TAE and RSAE amplitudes and will require significant development before ECH can be used in the control algorithm.

It is pointed out that the experiments presented here were carried out during the current ramp-up phase of the discharge to take advantage of an extensive body of work which has shown that a spectrum of AEs can be driven reliably and reproducibly during that period. The evolving current profile during the current ramp portion of the discharge, however, causes a large variation in discharge conditions and EP orbits

as well as the eigenmodes themselves. This transient situation makes the feedback control process difficult and can be the cause of the complicated phenomena observed when using ECH as an actuator. In the future, it is a priority to test the AE control system in the flat-top phase of steady state discharges, where multiple AEs have been shown to degrade performance significantly [8]. This is also an important step towards not only being a routine controller in the DIII-D PCS but becoming feasible for ITER. As for ITER the candidate real-time AE sensors and actuators are similar to DIII-D, i.e. sensor options include magnetic probes, the ECE system and interferometer/polarimetry diagnostics while possible actuators include ECH, neutral beam and applied 3D fields. Future work will also include real-time calculations of the classical neutron emission and incorporation of the ratio of measured to classical neutron emission as a feedback target. Because some level of AE activity can be observed before significant performance degradation occurs, it is expected that this ratio will be a more sensitive indicator when AE control is necessary.

Acknowledgments

The authors would like to express gratitude to Dr. John Ferron for his support of neutral beam modulation algorithm. The authors are also very grateful to Mr. Ben Penaflo for preparing the real-time ECE digitizer for the experiments. The authors want to thank Mr. Alan Hyatt and Dr. Michael Walker for their kind help and advice during the experiments. The authors would like to thank Dr. Xiaodi Du for calculations of the expected AE resonances. This work was supported by General Atomics under US Department of Energy contract DE-FC02-04ER54698.

Disclaimer

This report was prepared as an account of work sponsored by an agency of the United States Government. Neither the United States Government nor any agency thereof, nor any of their employees, makes any warranty, express or implied, or assumes any legal liability or responsibility for the accuracy, completeness, or usefulness of any information, apparatus, product, or process disclosed, or represents that its use would not infringe privately owned rights. Reference herein to any specific commercial product, process, or service by trade name, trademark, manufacturer, or otherwise, does not necessarily constitute or imply its endorsement, recommendation, or favoring by the United States Government or any agency thereof. The views and opinions of authors expressed herein do not necessarily state or reflect those of the United States Government or any agency thereof.

ORCID iDs

Wenhui Hu  <https://orcid.org/0000-0003-3420-2607>
 K.E.J. Olofsson  <https://orcid.org/0000-0001-9019-212X>
 W.W. Heidbrink  <https://orcid.org/0000-0002-6942-8043>

References

- [1] Gorelenkov N.N. et al 2014 *Nucl. Fusion* **54** 125001
- [2] Berk H.L. et al 1992 *Phys. Rev. Lett.* **68** 3563–6
- [3] White R.B. et al 2010 *Plasma Phys. Control. Fusion* **52** 045012
- [4] Todo Y. et al 2016 *Nucl. Fusion* **56** 112008
- [5] García-Muñoz M. et al 2010 *Phys. Rev. Lett.* **104** 185002
- [6] Sigmar D.J. et al 1992 *Phys. Fluids B* **4** 1506–16
- [7] Appel L.C. et al 1995 *Nucl. Fusion* **35** 1697
- [8] Heidbrink W.W. et al 2014 *Plasma Phys. Control. Fusion* **56** 095030
- [9] Holcomb C.T. et al 2015 *Phys. Plasmas* **22** 055904
- [10] Duong H.H. et al 1993 *Nucl. Fusion* **33** 749
- [11] Van Zeeland M.A. et al 2011 *Phys. Plasmas* **18** 056114
- [12] Collins C.S. et al 2017 *Nucl. Fusion* **57** 102018
- [13] Hawryluk R.J. 1999 *Phil. Trans. R. Soc. A* **357** 443–69
- [14] Zweben S.J. et al 2000 *Nucl. Fusion* **40** 91–149
- [15] Asunta O. et al 2012 *Nucl. Fusion* **52** 94014–7
- [16] Kurki-Suonio T. et al 2009 *Nucl. Fusion* **49** 095001
- [17] Collins C.S. et al 2016 *Phys. Rev. Lett.* **116** 1–5
- [18] Tsypin V.S. et al 1998 *Phys. Plasmas* **5** 7–9
- [19] Tsypin V.S. et al 1998 *Plasma Phys. Control. Fusion* **40** 665–8
- [20] Bruma C. et al 2003 *Plasma Phys. Control. Fusion* **45** 489–504
- [21] Wong K.L. et al 2004 *Phys. Rev. Lett.* **93** 040401
- [22] Snipes J.A. et al 2011 *Fusion Sci. Technol.* **59** 427–39
- [23] Snipes J.A. et al 2012 *Fusion Eng. Des.* **87** 1900–6
- [24] Yamamoto S. et al 2017 *Nucl. Fusion* **57** 126065
- [25] Petty C.C. et al 2015 *AIP Conf. Proc.* **1689** 090002
- [26] Van Zeeland M.A. et al 2009 *Nucl. Fusion* **49** 065003
- [27] Van Zeeland M.A. et al 2008 *Plasma Phys. Control. Fusion* **50** 035009
- [28] Van Zeeland M.A. et al 2016 *Nucl. Fusion* **56** 112007
- [29] Marchenko V.S. et al 2013 *Plasma Phys. Control. Fusion* **55** 052002
- [30] Garcia-Munoz M. et al 2015 *42nd EPS Conf. on Plasma Physics (Lisbon, Portugal, 22–26 June 2015)* (<http://ocs.ciemat.es/EPS2015PAP/pdf/P4.118.pdf>)
- [31] Nagaoka K. et al 2013 *Nucl. Fusion* **53** 072004
- [32] Pace D.C. et al 2017 *Nucl. Fusion* **57** 014001
- [33] Fredrickson E.D. et al 2017 *Phys. Rev. Lett.* **118** 265001
- [34] Bortolon A. et al 2013 *Phys. Rev. Lett.* **110** 265008
- [35] Kramer G.J. 2016 *Plasma Phys. Control. Fusion* **58** 085003
- [36] Garcia-Munoz M. et al 2017 *IAEA Technical Meeting on Energetic Particles in Magnetic Confinement Systems (Princeton, United States of America, 5–8 September 2017)* (https://nucleus.iaea.org/sites/fusionportal/Shared/Documents/EP_17th/5.09/I-2.pdf)
- [37] Marchenko V.S. 1993 *Nucl. Fusion* **33** 1871–5
- [38] Fredrickson E.D. et al 2015 *Nucl. Fusion* **55** 053012
- [39] Heidbrink W.W. et al 2007 *Phys. Rev. Lett.* **99** 245002
- [40] Van Zeeland M.A. et al 2012 *Nucl. Fusion* **52** 094023
- [41] Austin M.E. et al 2003 *Rev. Sci. Instrum.* **74** 1457–9
- [42] Van Zeeland M.A. et al 2006 *Phys. Rev. Lett.* **97** 1–4
- [43] Nazikian R. et al 2008 *Phys. Plasmas* **15** 056107
- [44] Weiland M. et al 2018 *Nucl. Fusion* **58** 082032